
**Liquid Crystals**
Publication details, including instructions for authors and subscription information:
http://www.informaworld.com/smpp/title~content=t713926090

# Liquid crystal droplet production in a microfluidic device

Benjamin D. Hamlington[a]; Benjamin Steinhaus[a]; James J. Feng[b]; Darren Link[c]; Michael J. Shelley[d]; Amy Q. Shen[a]
[a] Mechanical and Aerospace Mechanical Engineering, Washington University in St. Louis, St. Louis, USA [b] Chemical & Biological Engineering, University of British Columbia, Vancouver, Canada [c] Raindance Technologies, USA [d] Courant Institute of Mathematical Sciences, New York University, USA

**To cite this Article** Hamlington, Benjamin D. , Steinhaus, Benjamin , Feng, James J. , Link, Darren , Shelley, Michael J. and Shen, Amy Q.(2007) 'Liquid crystal droplet production in a microfluidic device', Liquid Crystals, 34: 7, 861 — 870
**To link to this Article: DOI:** 10.1080/02678290601171485
**URL:** http://dx.doi.org/10.1080/02678290601171485

*Liquid Crystals*, Vol. 34, No. 7, July 2007, 861–870



# Liquid crystal droplet production in a microfluidic device

BENJAMIN D. HAMLINGTON†, BENJAMIN STEINHAUS†, JAMES J. FENG‡, DARREN LINK§, MICHAEL J. SHELLEY¶ and AMY Q. SHEN†*

†Mechanical and Aerospace Mechanical Engineering, Washington University in St. Louis, St. Louis, MO 63130, USA
‡Chemical & Biological Engineering, University of British Columbia, Vancouver, BC V6T 1Z3, Canada
§Raindance Technologies, USA
¶Courant Institute of Mathematical Sciences, New York University, USA

(*Received 28 June 2006; in final form 16 September 2006; accepted 13 November 2006*)

Liquid crystal drops dispersed in a continuous phase of silicone oil are generated with a narrow distribution in droplet size in microfluidic devices both above and below the nematic-to-isotropic transition temperature. Our experiments show that the surface properties of the channels can be critical for droplet formation. We observe different dynamics in liquid crystal droplet generation and coalescence, and distinct droplet morphology on altering the microchannel surface energy. This is explained by the thermodynamic description of the wetting dynamics of the system. The effect of the nematic-to-isotropic transition on the formation of liquid crystal droplets is also observed and related to the capillary number. We also investigate how the nematic droplet size varies with the flow rate ratio and compare this behaviour with a Newtonian reference system. The effect of the defect structures of the nematic liquid crystal can lead to distinctly different scaling of droplet size in comparison with the Newtonian system. When the nematic liquid crystal phase is stretched into a thin filament before entering the orifice, different defect structures and numbers of defect lines can introduce scatter in the drop size. Capillary instabilities in thin nematic liquid crystal filament have an additional contribution from anisotropic effects such as surface gradients of bending stress, which can provide extra instability modes compared with that of isotropic fluids.



## 1. Introduction

Many phases of liquid crystalline materials exist, each distinguished by the spatial arrangements of the constituent liquid crystal molecules. The nematic phase is that most commonly used in commercial applications. Thermotropic liquid crystals remain in the nematic phase only within a specific temperature range; outside of this range, the material either becomes isotropic and loses its ordered structure, or assumes a much more structured phase such as the smectic phase. Liquid crystals can be engineered to have a large nematic temperature range and thereby great functionality.

Dispersions of nematic liquid crystal have unique optical and rheological properties. Examples of this are found in the interactions between water droplets dispersed in nematic liquid crystal [1], defect gels in cholesteric liquid crystals that are stabilized by particles [2] with enhanced elastic modulus, and electro-optically tunable scattering of light with polymer dispersed liquid crystals [3]. Typical methods for the generation of droplets in these dispersions result in a wide range of droplet size and shape. When the droplets are made sufficiently uniform in size they have a strong tendency to organize into a regular packing. The regularity of the packing and uniformity of droplet size can result in a modulation of the index of refraction that is sufficiently regular to achieve interference effects with coherent light [4]. This effect has applications for the high speed electrical modulation of optical diffraction properties. However, the technology needed to generate dispersions with a precisely controlled distribution of droplet sizes is currently very limited. Several methods have been suggested for uniform emulsification of two fluids, including micromachined combs, shearing the fluid between plates [5], phase separation [6], polymerization [7] and forcing droplets through a T-junction or flow-focusing geometry [8, 9]. While each of these proposed methods can produce emulsification, obtaining uniform size in a reproducible fashion remains a challenge. It would be advantageous to have a technology capable of precisely controlling droplet size and the distribution of sizes. This would allow for the tailoring of electro-optical properties and the large scale production of materials.

Microfluidics has emerged in recent years as a method of manipulating fluid at small length-scales

*Corresponding author. Email: aqshen@me.wustl.edu

*Liquid Crystals*
ISSN 0267-8292 print/ISSN 1366-5855 online © 2007 Taylor & Francis
http://www.tandf.co.uk/journals
DOI: 10.1080/02678290601171485

[10, 11], and in particular, for generating and manipulating droplets [8, 9, 12, 13]. In this work we present a microfluidic strategy for a more controlled generation of nematic liquid crystal droplets. We use a microfluidic system to create liquid crystal droplets of uniform size in a continuous phase of silicone oil. By altering the flow rates of the liquid crystal and silicone oil, uniformly dispersed droplets of liquid crystal can be formed within a microchannel. The two flow rates will also determine the size of the dispersed phase droplets. A similar method for droplet formation was developed by Umbanhowar *et al.* [14], which utilized a capillary pipette in a coflowing continuous phase. Droplets detached when the viscous stream forces of the continuous phase exceeded those of interfacial tension between the two phases. Fernandez-Nieves *et al.* used this method to create liquid crystal droplets in a continuous phase of water with polydispersity of less than 3% [15]. Our method is based on the same physical principle. But a primary advantage of using microfluidic channels is the ability to create a reproducible test set-up in which liquid crystal droplets of more uniform size and dispersion can be produced. Such a set-up also allows for certain parameters such as temperature and especially surface properties to be easily adjusted. The interaction between the liquid crystal phase, the silicone oil, and the confined geometry and bounding surfaces may have important implications for droplet coalescence and deformation after pinch-off at the orifice.

In this article, we report a new technique for making liquid crystal emulsion drops with a narrow distribution in droplet size, both above and below the nematic-to-isotropic phase transition temperature, by using a microfluidic device. Our experiments show that the surface properties of the microchannels can be critical for forming droplets. The effect of the nematic-to-isotropic transition on the formation of liquid crystal droplets is also observed and related to the capillary number. We observe that the presence of defect structures of nematic liquid crystal can lead to distinctly different droplet sizes and power law relations between droplet size and flow rate ratios in comparison with the Newtonian system.

## 2. Experiments

### 2.1. *Materials*

Thermotropic liquid crystal, 4′-pentyl-4-biphenylcarbonitrile (5CB), was purchased from Merck and used as received. Rai *et al.* [16] found that 5CB undergoes a crystal–nematic transition at approximately 21°C and a nematic–isotropic transition at approximately 35°C. Using an AR2000 stress-controlled rheometer with a cone and plate geometry (diameter 60 mm, cone angle 1°, truncation 29 μm), we verified these transitions using a temperature sweep with a shear rate of $100\,s^{-1}$, as illustrated in figure 1. This plot shows the dissipative portion of the complex viscosity $\eta'$ as a function of temperature. Since the storage modulus of 5CB is negligible, the dissipative portion of the complex viscosity is essentially the shear viscosity. A large jump in the shear viscosity occurs at 35°C due to the phase transition of the liquid crystal. The transition from the nematic phase to the isotropic phase is also observed optically using a polarizing microscope; see table 1 for detailed material properties.

### 2.2. *Experimental set-up*

The microfluidic channels were formed from polydimethylsiloxane (PDMS) using standard soft lithography techniques [17]. Both substrates were made of PDMS to ensure consistent properties on all four walls of the microchannel. Figure 2 shows the geometry of the microfluidic device. Similar designs were used by Anna *et al.* [18] and Ganan-Calvo and Gordillo [19]. The continuous phase is introduced into the two side wells, while the dispersed fluid flows through the centre channel of the system. Digital syringe pumps (Harvard Apparatus PHD 2000 Infusion pumps) are used to enforce a constant flow rate through each orifice. The three flows meet before entering a narrow channel that opens into the run-off channel. In an appropriate range of the flow rates, the centre fluid will pinch off to form droplets in the run-off channel. The 5CB liquid crystal (LC) was used as the dispersed phase and 20 cSt silicone oil was used as the continuous phase.

Droplet formation was tested in microchannels with different surface hydrophobicity. Although LC is not a water based solution, we borrow the terms *hydrophilicity* and *hydrophobicity* to refer to the affinity and repulsion between the PDMS substrate and the LC phase.

After forming the microdevice, the surface properties in the PDMS channels are hydrophobic. To change the PDMS surfaces from hydrophobic to hydrophilic, the channels were exposed to a plasma gas (using a Harrick Scientific plasma cleaner). Plasma exposure rearranges the terminal PDMS hydroxyl groups, increasing the surface free energy, and rendering the surface hydrophilic [20, 21, 22]. If the PDMS is allowed to be exposed to oxygen, the change in surface properties will gradually shift back over a period of one hour. However, if the PDMS slabs are immersed in a liquid, then the change in surface properties can be extended for up to 24 hours. We perform all experiments immediately after the surface treatment.

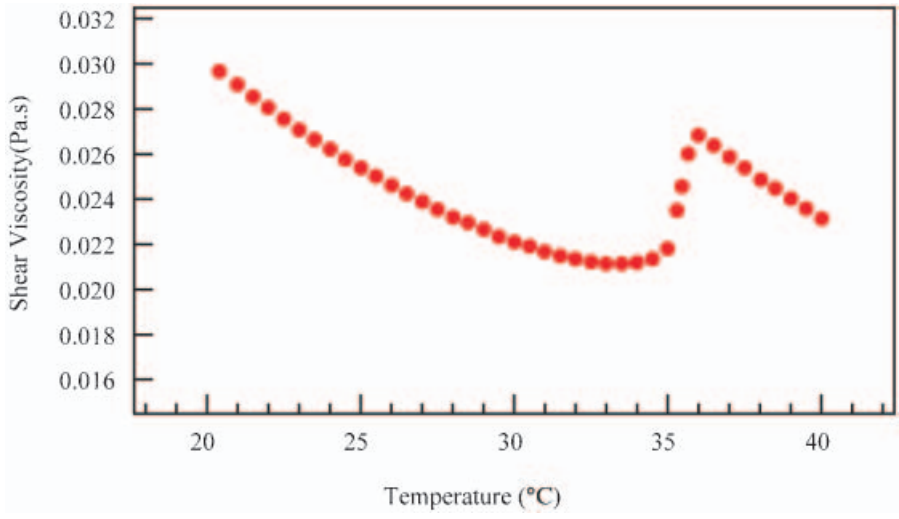


Figure 1. Rheology characterization of 5 CB under temperature sweep using an AR2000 rheometer. The shear viscosity is the dissipative part of the complex viscosity in small amplitude oscillation.



The hydrophobicity/hydrophilicity of a solid surface is usually expressed in terms of wettability, which can be quantified by contact angle measurements. Static contact angle is defined as the angle formed at the interface between the liquid and the substrate when we place a liquid droplet on a solid surface. The wettability of a surface by a fluid is controlled by both long range (van der Waals) force between the two media and short range interactions between molecules at the interface [23]. Low values of contact angle indicate that the drop fluid spreads well on the surface, while high values indicate poor wetting. The static contact angles of LC and silicone oil on the PDMS surface are measured by the sessile drop method (table 2 and figure 3) and are observed to change drastically when the hydrophobicity of the channel wall varies; see a more detailed discussion on surface hydrophobicity effects in the next section.

The temperatures of the channel and fluids were held at 23°C for one set of experiments and at 40°C for another set. At 23°C the LC is in the nematic phase, and at 40°C it is in the isotropic phase. In addition, the viscosity of the LC is roughly the same at these two temperatures. To maintain the temperature of the system at 40°C, we used the Instec STC200 temperature stage. In total, four different experimental conditions were tested by varying surface property and temperature. For each condition, the flow rates of the dispersed

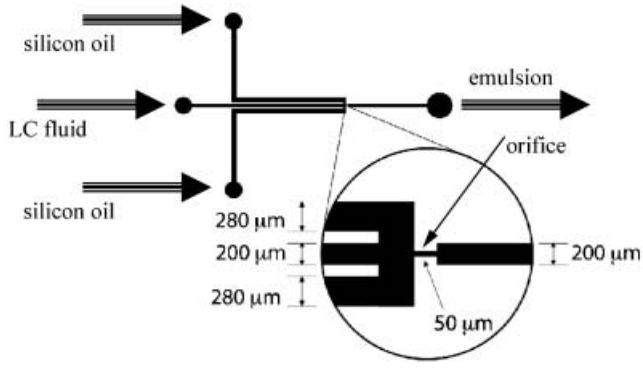


Figure 2. Microfluidic device used for droplet formation. The dispersed phase flows down the centre channel and pinches off at the orifice, while the continuous phase flows down the two outside channels.

Table 1. Material properties of 5 CB and silicone oil at 23°C and 40°C. $U$ is the average fluid velocity which can be determined by the flow rates of liquid crystal and silicone oil, and channel geometry. Capillary number ranges from $10^{-4}$ to $10^{-2}$ in our experiments.

| Property | 23°C | 40°C |
|---|---|---|
| LC Viscosity (mPa s) | 22.5 | 21.5 |
| Silicone oil Viscosity (mPa s) | 18.4 | 12.7 |
| Interfacial tension (with silicone oil) (mN m$^{-1}$) | 7.12 | 11.9 |
| Capillary number | $\approx 2.6 \times U$ | $\approx 1.1 \times U$ |

Table 2. Static contact angle measurements. Isotropic phase liquid crystal contact angle measurements were not conducted due to the inability to form droplets, hence the contact angle measurements would not provide any new information.

| Surface | Silicone oil in liquid crystal | Liquid crystal in silicone oil |
|---|---|---|
| PDMS (hydrophobic) | 45.6° | 134.4° |
| Treated PDMS (hydrophilic) | 143.0° | 37.0° |

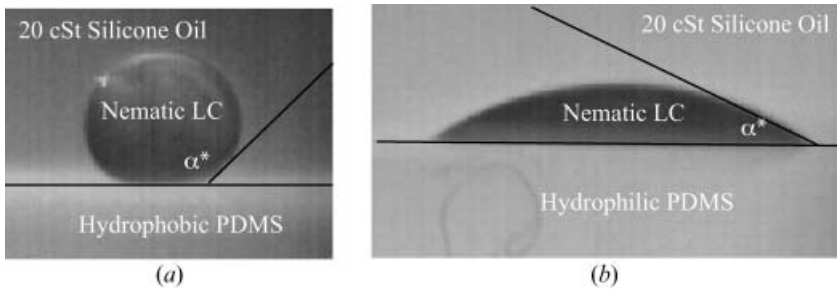


Figure 3. Images of liquid crystal droplets in contact with PDMS when immersed in silicone oil at room temperature. Image A shows the droplet in contact with hydrophobic PDMS; image B shows the droplet in contact with hydrophilic PDMS.

and continuous phases were varied in an attempt to understand the hydrodynamic conditions for droplet formation. Once the droplets were formed, their diameter was measured as a function of the dispersed and continuous phase flow rates.

## 3. Experimental results and discussion

### 3.1. *Phase diagrams*

Four phase diagrams have been generated by varying the flow rate of each fluid inside either hydrophobic or hydrophilic channels at two different temperatures, 23 and 40°C. This procedure allows us to focus on the effects of the surface properties and the nematic and isotropic properties of the LC. For each phase diagram, the flow rate of the dispersed phase ($Q_{lc}$ in the centre channel) ranges from 0.01 to 1.00 mL h$^{-1}$ while the flow rate of the continuous phase ($Q_o$ in the outer channels) is increased from either 0.01 or 0.03 to 1.00 mL h$^{-1}$. This systematic approach results in either 81 or 100 data points per phase diagram. After start of flow, we wait for 5 to 30 min for the system to pass its initial transient before recording its characteristic behaviour.

The four phase diagrams display four distinct flow patterns under different flow rate combinations: stratified flow, transient flow, unstable droplet formation, and stable droplet formation. *Stratified flow* of the continuous and dispersed phase consists of the two fluids travelling in separate streams in a stable fashion, and makes up the largest portion of all of the phase diagrams (see figure 4). As the flow rate of the silicone oil is increased, stratified flow occasionally gives way to a *transient flow* behaviour, where LC flow in the centre channel breaks off into silicone oil (side channels) in a periodic flapping mode. With increasing flow rates of both phases, the LC phase is stretched into thin filaments that can pinch off when passing through the orifice to form droplets in the downstream channel. Depending on the flow rates, the system can take as long as 30 min to pass transient state in this regime. For some flow rate combinations, *unstable droplet formation* was observed (see figure 4 B), where droplet formation tends to be random and droplet coalescence occurs in the downstream of the channel. With certain flow rates and the appropriate surface type, *stable droplet formation* can be achieved. In this regime, droplets are produced in a perfectly periodic fashion with uniform size droplets in most cases.

The phase diagrams in figure 4 A and B show the results for nematic droplet formation experiments at room temperature, 23°C. As the phase diagrams illustrate, it is relatively easy to form droplets when the surface properties are hydrophobic but much more difficult when the surface properties are changed to hydrophillic. Phase diagram A (hydrophobic surface) shows a large region of stable droplet formation, while phase diagram B (hydrophilic surface) has only unstable droplet formation.

We can explain the above observations based on the thermodynamic description of the wetting dynamics of two immiscible fluids interacting with a solid substrate. Here, we will focus on the nematic LC droplet formation. Interfacial tension between silicone oil and nematic LC $\gamma_{ol}$ and equilibrium contact angle $\alpha^*$ between LC phase and the substrate can be measured experimentally (given in table 2 and figure 3). The large contact angle between the LC and hydrophobic PDMS is displayed in image A of figure 3. When the channel is treated with plasma gas to become hydrophilic, the contact angle of the LC in contact with the PDMS is greatly reduced and it becomes difficult to form droplets. We can deduce the surface energy difference between the PDMS/silicone oil and PDMS/LC by using a modified Young's equation [24] that is applicable for both nematic and isotropic LC:

$$\gamma_{ol}\cos(\alpha^*) = \gamma_{so} - \gamma_{sl} + B^{bl}\sin(\alpha^*) \qquad (1)$$

where $\gamma$ represents the free energy per unit surface area, and the subscripts o, l, s represent continuous (silicone oil), dispersed (both nematic and isotropic LC), and solid phases respectively. The bending force term,

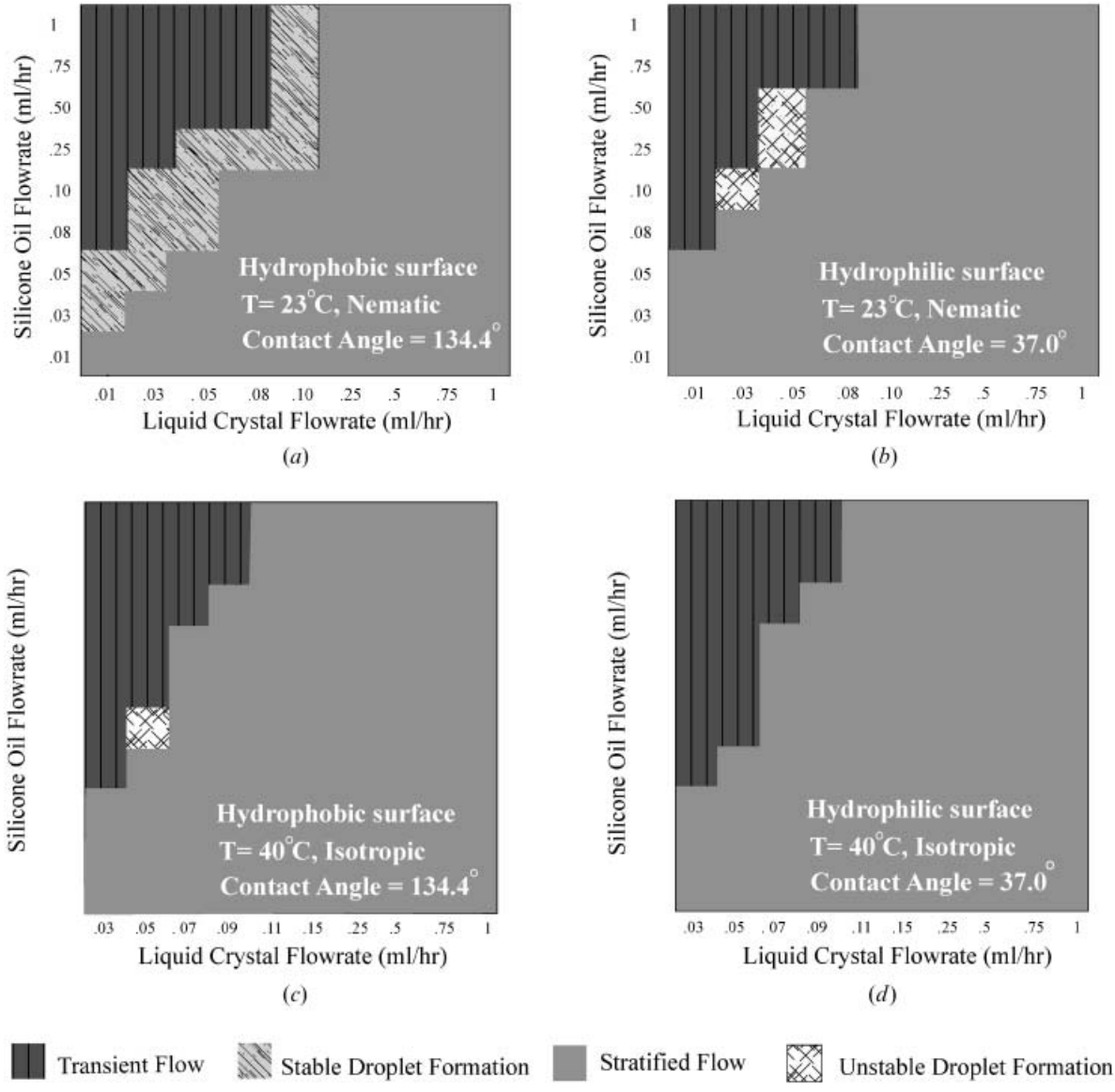


Figure 4. Phase diagrams for liquid crystal in both the nematic phase (A and B) and the isotropic phase (C and D). Liquid crystal is used as the dispersed phase, while 20 cSt silicone oil is used as the continuous phase. The channel properties were hydrophobic in A and C, and hydrophilic in B and D.

$B^{bl}\sin(\alpha^*)$, originates from the surface anchoring between a nematic LC and PDMS surface and disappears when the LC becomes isotropic. Furthermore, for nematic LC, the interfacial tension $\gamma_{ol}$ in equation (1) has contributions from both isotropic and nematic ordering (due to anisotropic anchoring energy). When the equilibrium contact angle of the LC droplet phase in contact with PDMS is greater than 90°, Young's equation yields $\gamma_{so}<\gamma_{sl}-B^{bl}\sin(\alpha^*)$. Thermodynamically, more energy is required for the LC phase to be in contact with the channel walls [25]. As a consequence, the LC does not wet the PDMS well, and is more likely to detach itself from the channel walls and form droplets. This argument agrees well with the experimental observation that nematic LC droplets form more easily for hydrophobic PDMS surfaces. On the other hand, for hydrophilic PDMS surface, the inequality $\gamma_{so}>\gamma_{sl}-B^{bl}\sin(\alpha^*)$ means that LC is more likely to attach to microchannel surfaces, such as the channel side walls and the bottom and the ceiling of the channels (see figure 5). In this case, it will be harder for the LC to detach from the walls and eventually break up into droplets.

When the LC was heated above the nematic-to-isotropic transition temperature, droplet formation became very difficult, as displayed in figure 4 C and

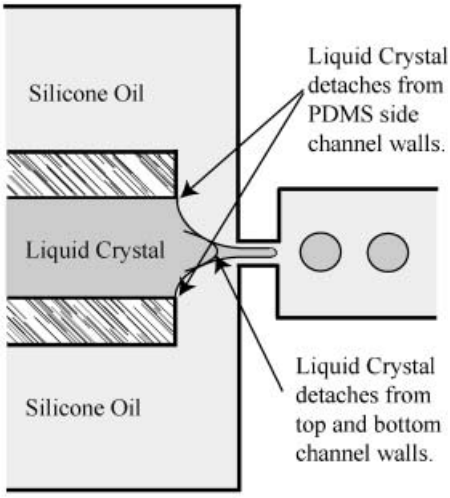


Figure 5. Schematic drawing of possible contact regions of liquid crystal phase with respect to PDMS walls that is related to surface hydrophobicity.



D. Only unstable droplet formation for a very small range of flow rates occurred regardless of the surface properties. This effect can be understood by examining the capillary and viscous forces between the LC and oil phases inside the microchannel. If we view the drop formation as a result of the viscous force overcoming the capillary force, we may define a capillary number as $Ca=\eta_o U/\gamma_{ol}$, with $\eta_o$ being the shear viscosity of the silicone oil. As given in table 1, the interfacial tension $\gamma_{ol}$ between the LC and the silicone oil is higher when the LC is in the isotropic phase. This trend does not follow the Eötvös rule [26], $\gamma_{ol}\approx 2.12(T^*-T)/\rho^{3/2}$, where $\rho$ is the density of LC, and $T$ and $T^*$ are the temperature and critical temperature of the LC respectively. The LC viscosity is more or less the same at 23°C as at 40°C, while the viscosity of the silicone oil decreases by a factor of 1.5 with that temperature increase. The higher $\sigma$ and lower $\eta_o$ at 40°C yield a capillary number less than half that at 23°C for the same flow rates. Thus, droplet formation will occur much more readily in the latter case, where the LC is in the nematic phase. In addition, the capillary force of nematic liquid crystals contains both isotropic and anisotropic contributions. Cheong and Rey [27] theoretically studied the capillary instabilities of thin nematic LC filaments and found that in a nematic phase, anisotropic effects from surface gradients of bending stress can provide additional instability modes compared with that of isotropic fluids. Such a mechanism may have played a role in facilitating drop formation when the LC is in the nematic phase. Finally, we note that the particulars of nematic anchoring at the channel wall, e. g. strong or weak, will introduce a length-scale—the extrapolation length [28] — into any detailed understanding of droplet production. How the extrapolation length interacts with droplet production under the influence of temperature and phase dependence [29], and especially how the strength of anchoring might be manipulated, are likely to be very interesting avenues of research. A more detailed study on anchoring strength and extrapolation length will be carried out in the future.

### 3.2. *Interfacial morphology*

Two flow instability regimes have been identified in previous experiments on Newtonian droplet formation in a flow-focusing device [30, 31]. The dripping regime occurs at relatively low flow rates and is characterized by periodic formation of highly uniform spherical droplets. As the flow rates increase, a transition to the jetting regime occurs, characterized by a jet extending downstream from the orifice with droplet formation at the tip of the jet [31].

Based on experimental observations, LC droplets form mainly in its nematic phase, therefore we will focus on the discussion of interfacial morphology of nematic LC droplets. At small flow rates of both LC and silicone oil phases, droplet formation is in the dripping regime (see figure 6). The flow is focused due to the strong contraction upstream of the orifice, which stretches the nematic LC into a filament inside the orifice. When the LC exits the orifice, expansion occurs that decelerates the flow, and the interfacial tension creates a spherical bulb of LC at the tip of the filament. The pinch-off of the nematic LC droplet occurs under the competition of viscous drag of the stretching filament of the LC phase, capillary forces and elastic curvature force. Note that capillary force contains both isotropic and anisotropic contributions for nematic liquid crystals.

Once the droplet has pinched off, the whole process repeats itself. In the dripping regime, we observe that the droplet size tends to be quite uniform and sometimes follow periodic production rates, but the pattern of drop formation varies with the flow rates. In figure 6 A, droplets of three sizes formed: a main droplet, a secondary droplet, and a very small satellite droplet. In figure 6 B, doublets were formed. Finally, figure 6 C shows a single stream of uniform nematic phase liquid crystal droplets forming at the orifice. At certain flow rate combinations, we also observe distinct defect lines when liquid crystal enters the orifice, and internal defect structures inside the nematic droplets (see figure 6 C).

With increasing flow rates of both phases, the dripping regime gives way to a jetting regime [31], which features a long jet that stretches downstream (figure 7). Jetting is a consequence of the increased flow

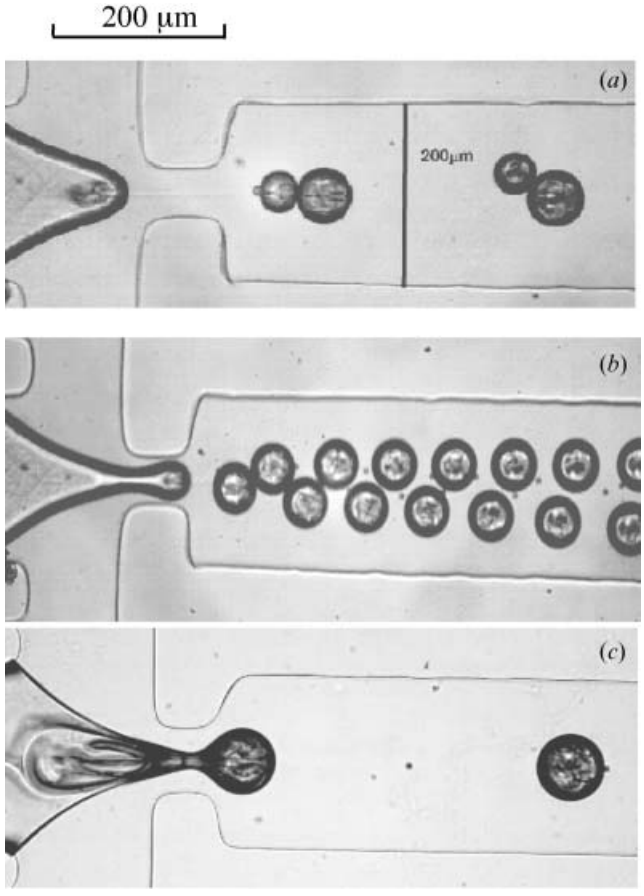


Figure 6. Nematic LC droplet formation in the dripping regime. A: nematic LC primary, secondary, and a satellite droplet pinching off at the orifice and travelling downstream. Flow rate of liquid crystal is $0.002\,\mathrm{ml\,h^{-1}}$, while flow rate of silicone oil is $0.02\,\mathrm{ml\,h^{-1}}$. B: nematic LC drops arrange themselves into two lines that move downstream of the orifice. Flow rate of liquid crystal is $0.003\,\mathrm{ml\,h^{-1}}$, while flow rate of silicone oil is $0.04\,\mathrm{ml\,h^{-1}}$. C: a single stream of nematic LC droplets forming at the orifice. Flow rate of liquid crystal is $0.001\,\mathrm{ml\,h^{-1}}$ while the flow rate of the silicone oil is $0.05\,\mathrm{ml\,h^{-1}}$.

rates that force the filament to travel at a greater rate. Unlike in the dripping regime, droplets do not form at the orifice, but instead form at the tip of the jet farther downstream. In general, the length of the jet will increase with increasing flow rates of the LC and silicone oil phases. Meanwhile, the jet becomes quite thick and produces larger droplets than in the dripping regime.

Drop formation in the jetting regime is due to capillary instability where capillary wave form can be discerned in the top image of figure 7. Cheong and Rey [27] studied the capillary instabilities in thin nematic liquid crystal fibres by taking account of nematic LC orientation and the anisotropic contribution to surface energy. They predicted that when the nematic orientation is along

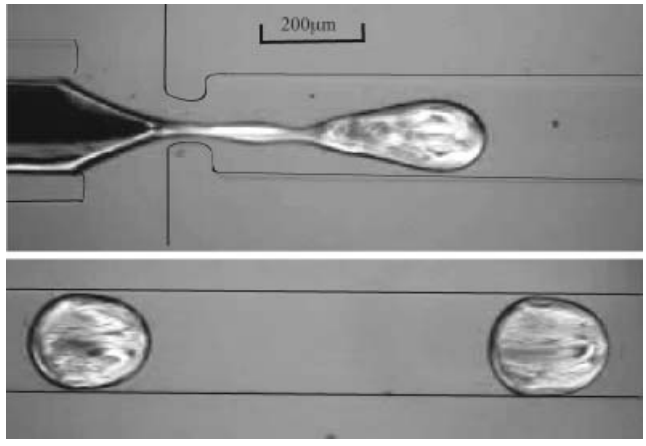


Figure 7. Liquid crystal droplet in the jetting regime pinching off after the orifice and travelling downstream. Bottom image shows droplets travelling downstream from the orifice. Flow rate of liquid crystal is $0.08\,\mathrm{ml\,h^{-1}}$, while flow rate of silicone oil is $0.25\,\mathrm{ml\,h^{-1}}$.

the filament direction, capillary instabilities can be axisymmetric. The elongation of the jet should have aligned the LC molecules into the flow direction, and the subsequent axisymmetric instability and drop pinch-off are consistent with the theory. The bottom image in figure 7 shows the nematic LC droplets travelling downstream from the orifice, and droplets are slightly distorted from spherical.

We also observed that nematic droplets do not coalesce easily after they are pinched off and flow downstream. This observation concurs with a recent report by Heppenstall-Butler *et al.* [32] that when the emulsion size is greater than the ratio of Frank elastic energy over surface anchoring energy (of the order of 10 to 100 μm), the topological charge can prevent droplet coalescence.

### 3.3. *Droplet size*

By varying the flow rates of the dispersed and continuous phases, the size of the droplets can be altered in a controlled manner. The ability to control the size of the LC droplets has important implications to many emerging technologies. Figure 8 plots the diameter of LC droplets $d$ scaled with the orifice width $a$ against the flow rate ratio between the LC dispersed phase and the continuous phase silicone oil. The experimental data were taken at 23°C with hydrophobic PDMS surfaces under both dripping and jetting regimes. For these measurements, the droplets were assumed to be spherical, based on in-plane measurements [9].

Figure 8 illustrates that for higher flow rate ratios and thus lower silicone oil flow rate, the droplet size

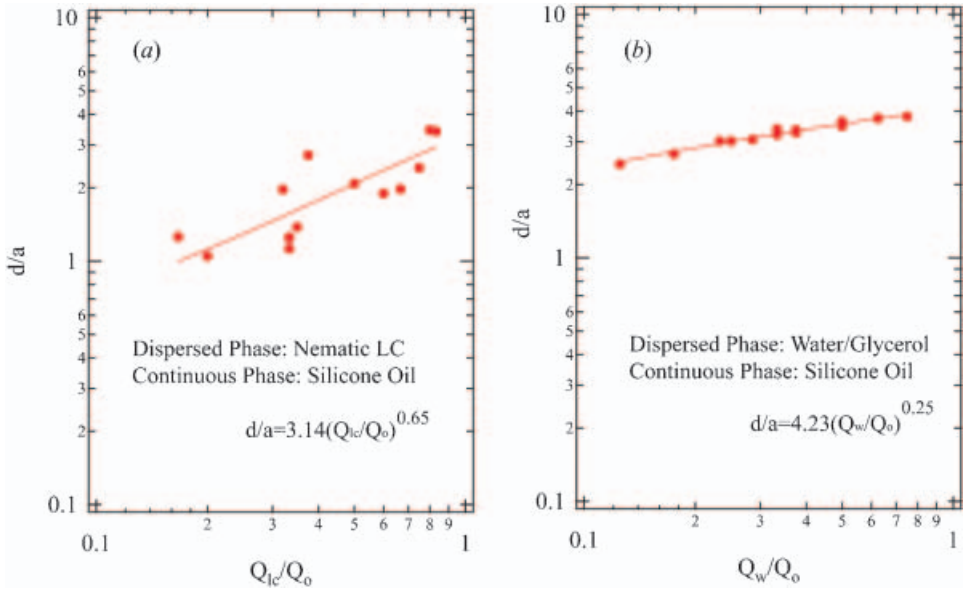


Figure 8. The ratio of droplet diameter to orifice width plotted versus the ratio of the dispersed phase flow rate to the continuous phase flow rate. A shows the results with liquid crystal as the dispersed phase and silicone oil as the continuous phase. The data cover both dripping and jetting regimes and the transition occurs roughly at $Q_{lc}/Q_o \approx 0.3$. B shows the results with a water/glycerol solution as the dispersed phase and silicone oil as the continuous phase. Below both figures is the log–log plot of the data. The surface properties of the channel were hydrophobic.



tends to be larger. As the flow rate of the LC decreases and the silicone oil flow rate increases, the droplet size decreases. This is expected since for higher silicone oil flow rates, the shearing effect on the LC phase is larger, and droplets will pinch off before reaching a significant size. Furthermore, we also observed a power law relationship between nematic LC drop size and flow rate ratios:

$$\frac{d}{a} = 3.14\left(\frac{Q_{lc}}{Q_o}\right)^{0.65} \qquad (2)$$

with $d$ the LC droplet size, $a$ the orifice width, $Q_{lc}$ the liquid crystal flow rate, and $Q_o$ the silicone oil flow rate.

As illustrated in figure 8 A, a relatively large amount of scatter (in a power law relation) of droplet size with respect to flow rate ratio was observed in the data obtained with the nematic LC and oil. In order to determine if this scatter was due to the experimental set-up and performance error or was a contribution from the nematic structure of the LC phase, measurements were made with aqueous solution (dispersed phase) and oil (continuous phase) as a Newtonian reference system. We kept the oil phase the same while choosing the aqueous solution as a mixture of water and glycerol to achieve a viscosity ratio of 1.1, the same ratio as the nematic liquid crystal versus 20 cSt oil. The interfacial tension between oil and water/glycerol mixture was measured to be $3.0\,\mathrm{mN\,m^{-1}}$ while the interfacial tension between nematic LC and oil was measured to be $7.1\,\mathrm{mN\,m^{-1}}$. With this Newtonian reference system, the measured droplet size is plotted in figure 8 B. Two interesting observations can be made.

First, with the Newtonian reference system, we obtained a slope of 0.25 for the droplet size versus flow rate ratios with less data scatter (see figure 8 B).Ward *et al.* [9] performed similar droplet pinch off experiments with deionized water and 34.5 cSt mineral oil as dispersed and continuous phases in a similar flow-focusing design. Despite the difference of viscosity ratio between the Ward system and our Newtonian reference experiments, their data also showed a slope of 0.25 that is in good agreement with our experiments. This observation leads us to conclude that the geometry and experimental error are not the cause for the scattering in the LC droplet data. Rather, the nematic LC structure may be responsible.

Secondly, we note that the nematic LC droplet size tends to be smaller at the same flow rate ratios when compared with the aqueous droplets. For a Newtonian system, droplet pinch-off dynamics and the drop size depend on a balance between viscous and capillary forces. For nematic LC droplets, an additional parameter is the elastic force due to orientational distortion. Note also that the nematic LC capillary force contains both isotropic and anisotropic contributions. These additional factors related to the nematic LC structures

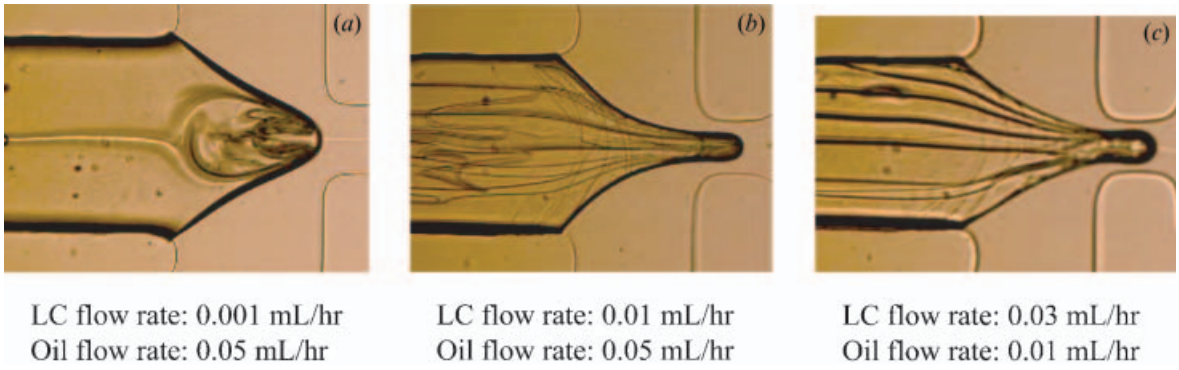


Figure 9. Images displaying the presence of defects with different defect strengths when the nematic liquid crystal filament is stretched into the orifice.

can lead to droplet sizes and power law indices that differ from their Newtonian counterparts.

Further to investigate the idea that nematic order may influence drop formation in liquid crystals, we show in figure 9 three snapshots of the defect structure inside the nematic phase. While the nematic LC phase is stretched into a thin filament before entering the orifice, we observe defect lines of different density and structure [33] at different flow rates. Conceivably, the characters of the defects depend on the upstream flow history, and may evolve during the course of an experiment. Therefore, they may impart a stochasticity to the process, and produce the noisy data for drop size with respect to flow rate ratios. In short, the nematic droplet size depends not only on the flow rate ratio of the two phases, but also on the nematic defect structures during the flow.

## 4. Conclusions

In this experimental study, we used a microfluidic flow-focusing device to produce liquid crystal droplets of controlled sizes. For the parameter ranges examined, the main results may be summarized as follows.

(1) Drop formation in the microfluidic channel depends on the affinity between the liquid crystal phase and the channel walls. Hydrophobicity greatly facilitates drop formation. In contrast, hydrophilicity hinders the detachment of the liquid crystal phase from the walls and the subsequent drop formation.

(2) Drop formation also depends on the flow rates of the two components. The dripping regime prevails for lower flow rates, and transforms to the jetting regime as the flow rates increase. The drop size follows a power law with respect to the liquid crystal-to-oil flow rate ratio.

(3) Drop size is strongly influenced by the molecular orientation and defect structure within the liquid crystal phase. Compared with their Newtonian counterpart, the liquid crystal drops are smaller, follow a different power law in terms of the flow rate ratio, and exhibit much greater variation in size with respect to the flow rate ratio. These may be explained by the anisotropic interfacial tension and the defect lines that modify the capillary instability that leads to drop pinch-off.

(4) We have also noted that liquid crystal drops form much more readily in the nematic phase (at a lower temperature) than in the isotropic phase (at a higher temperature). But the difference may have more to do with the interfacial tension and change in viscosity with temperature.

## Acknowledgements

We sincerely thank Professors Eliot Fried and Alejandro Rey for helpful discussion related to this work. J. J. F. acknowledges partial support by the Petroleum Research Fund, administered by the American Chemical Society, the NSERC, the Canada Research Chair program, the Canada Foundation for Innovation and the NSFC (No. 20490220). A. Q. S. wishes to thank the National Science Foundation (No. 0645062) for their support.

## References

[1] P. Poulin, H. Stark, T.C. Lubensky, D.A. Weitz. *Science*, **275**, 1770 (1997).
[2] M. Zapotocky, L. Ramos, P. Poulin, T.C. Lubensky, D.A. Weitz. *Science*, **283**, 209 (1999).
[3] P.S. Drzaic. *Liq. Cryst.*, **3**, 1543 (1988).
[4] A. Fernandez-Nieves, D.R. Link, D. Rudhardt, D.A. Weitz. *Phys. Rev. Lett.*, **92**, 105503 (2004).
[5] J.C. Loudet, H. Richard, J. Sigaud, P. Poulin. *Langmuir*, **16**, 6724 (2000).
[6] J.C. Loudet, P. Barois, P. Poulin. *Nature*, **407**, 611 (2000).
[7] D. Harrison, M.R. Fisch. *Liq. Cryst.*, **27**, 737 (2000).

[8] D.R. Link, S.L. Anna, D.A. Weitz, H.A. Stone. *Phys. Rev. Lett.*, **92**, 5 (2004).
[9] T. Ward, M. Faivre, M. Abkarian, H.A. Stone. *Electrophoresis*, **26**, 3716 (2005).
[10] H.A. Stone, A.D. Stroock, A. Ajdari. *Ann. Rev. Fluid Mech.*, **36**, 381 (2004).
[11] H.A. Stone, S. Kim. *AIChE J.*, **47**, 1250 (2001).
[12] J. Atencia, D.J. Beebe. *Nature*, **437**, 648 (2005).
[13] M. Joanicot, A. Ajdari. *Science*, **309**, 887 (2005).
[14] P.B. Umbanhowar, V. Prasad, D.A. Weitz. *Langmuir.*, **16**, 347 (2000).
[15] A. Fernandez-Nieves, G. Cristobal, V. Garces-Chavez, G.C. Spalding, K. Dholakia, D.A. Weitz. *Adv. Mater.*, **17**, 680 (2005).
[16] P.K. Rai, M.M. Denn, C. Maldarelli. *Langmuir*, **19**, 7370 (2003).
[17] Y.N. Xia, G.M. Whitesides. *Ann. Rev. mater. Sci.*, **28**, 153 (1998).
[18] S.L. Anna, N. Bontoux, H.A. Stone. *Appl. Phys. Lett.*, **82**, 364 (2003).
[19] A.M. Ganan Calvo, J.M. Gordillo. *Phys. Rev. Lett.*, **87**, 274501 (2001).
[20] J. Kim, M.K. Chaudhury, M.J. Owen, T. Orbeck. *J. colloid interface Sci.*, **244**, 200 (2001).
[21] H. Hillborg, J. Ankner, U. Gedde, G. Smith, H. Yasuda, K. Wikstrom. *Polymer*, **41**, 6851 (2000).
[22] J. McDonald, G. Whitesides. *Acc. chem. Res.*, **35**, 491 (2002).
[23] P.G. de Gennes. *Rev. mod. Phys.*, **57**, 827 (1985).
[24] A.D. Rey. *J. chem. Phys.*, **111**, 7675 (1999).
[25] R. David. *Thermodynamics of Materials*. John Wiley, (1994).
[26] A.W. Adamson, A.P. Gast. *Physical Chemistry of Surfaces*, 5th Edn, John Wiley (1997).
[27] A. Cheong, A.D. Rey. *Phy. Rev. E*, **64**, 041701 (2001).
[28] J. Prost, P.G. de Gennes. *Physics of Liquid Crystals*, 2nd Edn, Oxford Science (1995).
[29] F. Vandenbrouck, B. Bardon, M. Valignat, A. Cazabat. *Phys. Rev. Lett.*, **81**, 610 (1998).
[30] A.S. Utada, E. Lorenceau, D.R. Link, P.D. Kaplan, H.A. Stone, D.A. Weitz. *Science*, **308**, 537 (2005).
[31] C. Zhou, P. Yue, J.J. Feng. *Phys. Fluids*, **18**, 092105 (2006).
[32] M. Heppenstall-Butler, A.M. Williamson, E.M. Terentjev. *Liq. Cryst.*, **32**, 77 (2005).
[33] A.D. Rey, M.M. Denn. *Annu. Rev. Fluid Mech.*, **32**, 233 (2002).